catalysts

MDPI

Article

Contributions of Washcoat Components in Different Configurations to the NO_X and Oxygen Storage Performance of LNT Catalysts

Can Özyalcin [1,2,*], Peter Mauermann [1,2], Jürgen Dornseiffer [2,3], Stefan Sterlepper [1,2], Marco Günther [1,2] and Stefan Pischinger [1,2]

[1] Chair of Thermodynamics of Mobile Energy Conversion Systems (TME), RWTH Aachen University, 52072 Aachen, Germany
[2] Center for Automotive Catalytic Systems Aachen (ACA), RWTH Aachen University, 52072 Aachen, Germany
[3] Institute of Energy and Climate Research: Materials Synthesis and Processing (IEK-1), Forschungszentrum Jülich, 52425 Jülich, Germany
* Correspondence: oezyalcin_c@tme.rwth-aachen.de; Tel.: +49-241-80-48004

Abstract: In addition to SCR systems, lean NO_X traps (LNTs) are also used for exhaust aftertreatment of lean burn internal combustion engines to sustainably reduce NO_X emissions. Modern LNTs consist of different functional compounds to maximize the performance during NO_X storage and regeneration. Based on the material analysis of a serial production LNT, PGM loaded BaO, Al_2O_3, $MgAl_2O_4$, and CeO_2 were identified as the main base materials. In this paper, the NO_X storage capacity (NSC) of these compounds is investigated both as single catalysts and as physical mixtures to identify possible synergistic effects. Therefore, commercially available support materials were loaded with Platinum and tested in granular form under realistic conditions. To optimize the performance by reducing the diffusion pathways for NO_X molecules during storage, PGM, BaO, and Ceria were combined in a composite by the incipient wetness impregnation of alumina. As a result, the temperature dependent NSC of the commercial LNT could be reached with the $Pt/Rh/Ba_{10}Ce_{25}/Al_2O_3$ infiltration composite, while reducing the oxygen storage capacity by about 45%. Without the additional Rhodium coating, the low-temperature NSC was insufficient, highlighting the important contribution of this precious metal to the overall performance of LNTs.

Keywords: exhaust gas aftertreatment; NOx aftertreatment; lean NO_X trap; NOx storage catalyst; composites; synergistic effect; oxygen storage capacity

Citation: Özyalcin, C.; Mauermann, P.; Dornseiffer, J.; Sterlepper, S.; Günther, M.; Pischinger, S. Contributions of Washcoat Components in Different Configurations to the NO_X and Oxygen Storage Performance of LNT Catalysts. *Catalysts* **2022**, *12*, 953. https://doi.org/10.3390/catal12090953

Academic Editors: Fan Lin and Jong-Ki Jeon

Received: 29 July 2022
Accepted: 24 August 2022
Published: 26 August 2022

1. Introduction

To reduce the overall greenhouse gas emissions and thus limit the increase in the global average temperature to below 2 °C, special measures are needed particularly for the internal combustion engines. One of the main approaches in the improvement of modern internal combustion engines is to increase the efficiency in order to reduce fuel consumption and carbon dioxide emissions. In this context, lean burn combustion concepts have the greatest potential. However, their oxygen-rich exhaust gases pose a major challenge in terms of effective NO_X reduction to comply with the global pollutant emission standards. Hence, catalytic exhaust gas aftertreatment remains a key technology for an effective NO_X abatement of lean operating internal combustion engines.

The two main challenges in NO_X reduction are the high conversion requirement under high speed and load conditions, as they occur in real driving emissions (RDE) cycles, and the emission reduction at low exhaust gas temperatures, as they occur in urban traffic and at cold start conditions. The two most prominent systems for catalytic NO_X reduction are the LNT (lean NO_X trap) catalyst and the SCR (selective catalytic reduction) catalyst [1]. Current trends are leading mainly to combined systems [2]. The term SCR

refers to continuously operating DeNOx systems in automotive exhaust gas aftertreatment, in which NO_X is selectively reduced even under high oxygen concentrations. The state-of-the-art SCR system used in automotive applications is the NH_3-SCR. Here, a urea–water solution is injected into the exhaust gas upstream of the catalytic converter and decomposes to CO_2 and NH_3. The ammonia then reduces the NO_X to N_2 on the catalyst surface. The SCR process was established primarily in the commercial vehicle sector and in medium to high class passenger cars [3,4].

LNTs are discontinuously operating NO_X reduction systems by working alternately in lean and rich operating conditions of the engine and are mainly used in light commercial vehicles. Compared to SCR catalysts, LNTs have advantages in terms of package space, weight, and price; and also show enhanced low-temperature performance. Therefore, they are the preferred first NO_X aftertreatment component downstream of the engine for small class vehicles [1]. In the 1990s, Toyota researchers introduced the first LNT technology [5]. In principle, the LNT is very similar to the three-way catalyst (TWC) used for stoichiometric operating gasoline engines. The main difference is the duration of the lean ($\lambda > 1$) and rich ($\lambda < 1$) conditions. A TWC is applied usually for shorter lean and rich cycling durations between 0.5 and 3 s, whereas LNTs are able to store NO_X during longer lean periods between 60 and 120 s. This difference impacts the capacity of the chemisorbed storage of NO_X molecules. Once the storage sites are full, the LNT has to be regenerated during a relatively longer rich operating phase, which takes between 5 and 20 s. Then, the stored NO_X is reduced under sub-stoichiometric conditions mainly with the reductants hydrogen (H_2), carbon monoxide (CO) and unburnt hydrocarbons (HC) in the exhaust gas.

A review of the literature has shown that the actual LNT technologies exhibit a combination of a wide spectrum of different catalytic materials [6–8]. In general, LNT catalysts consist of Platinum Group Metals (PGMs), NO_X storage components and support metal oxides, the simple state-of-the-art catalyst being $Pt/BaO/Al_2O_3$ [6]. Modern commercial LNTs contain hydrotalcite derived Mg spinel ($MgAl_2O_4$), ceria (CeO_2), alumina (Al_2O_3) and barium oxide (BaO), loaded with platinum (Pt), palladium (Pd) and rhodium (Rh) for different functionalities within the washcoat [9]. Alkaline earth metals are chosen due to their high basicity and thus NO_X trapping performance [10]. PGMs are used generally in a very low amount. As reviewed in previous works, Pt and Pd have been established as highly active oxidation catalysts [10,11], while Rh mainly supports reduction activities under rich conditions [7]. Bimetallic applications of LNTs, such as Pt/Rh or Pd/Rh, can also be found in the literature [12,13].

The main limiting factor in the LNT activity is the NO_X storage capacity (NSC). The alkaline earth storage sites, such as barium oxides (BaO), are more efficient at adsorbing NO_2 than NO. Therefore, the NO oxidation is an essential step for the catalyst's performance and takes place primarily on Pt sites, which can be controlled either kinetically or thermodynamically under lean conditions [14,15]. At low temperatures, kinetic limitations regarding the performance of the catalytic material are dominant, such that the NO to NO_2 oxidation cannot reach its thermodynamic equilibrium. At temperatures above 350 °C, the equilibrium could easily be reached. In the light of these two limitations, a maximum for the NO_2/NO_X ratio occurs in a temperature range around 300 °C for de-greened $Pt/BaO/Al_2O_3$ based catalysts [16]. At temperatures higher than 600 °C, the equilibrium of the NO oxidation is mostly on the NO side.

Further important reactions occur on the ceria (CeO_2) sites, which is normally coated with platinum. Its main function within the catalyst is to promote the water gas shift (WGS) reaction in the rich phases to produce additional hydrogen for NO_X reduction [17–19]. Another function of platinized ceria is to enhance NO_X storage during lean phases. For middle temperature range between 250 °C and 350 °C, ceria promotes nitrate formation and thus the NSC of the BaO sites [20]. Catalysts with a significant ceria amount in the washcoat show an enhanced oxidation and diffusion behavior at low temperatures resulting in a better storage performance. Moreover, ceria itself can also store NO_X [21,22]. For these reasons, ceria is an essential component for LNTs. In addition to the well-known

conventional LNT materials, further materials, e.g., perovskites [23–26] or hydrotalcite-derived spinel compounds ($MgAl_2O_4$) [7,27–31], can be used as alternative NO_X storage materials in particular for low temperatures. All these materials have both unique and synergistic functions in LNTs.

Publications on the NO_X storage performance of conventional and alternative materials or mixtures of them have been investigated under a great variety of boundary and test conditions [32–36]. These different experimental setups make it difficult to directly compare the results and to investigate the synergistic effect of the washcoat components, which is crucial for the storage performance of a fully formulated commercial LNT.

Within this work, the temperature-dependent NO_X adsorption behavior for all individual washcoat components of modern LNTs, as well as the interactions and possible synergistic effects of physical mixtures of them, were systematically investigated under realistic test conditions in granulized form. The results are compared with the performance of a commercially available LNT from series production as a reference. To optimize the performance, BaO and ceria were combined in a composite by the incipient wetness impregnation (IWI) of alumina loaded with different PGMs and investigated to improve the NO_X storage capacity by reducing the diffusion distance of NO_X molecules during storage. Finally, a possible tailored catalyst design for lean burn combustion engines was discussed.

2. Results

2.1. NO_X Storage Performance

NO_X storage assessments were performed on both individual materials as well as physical and chemical mixtures thereof under realistic conditions in a temperature range between 150 °C and 450 °C on the laboratory gas test bench. For these measurements, granules in the size range of 1–1.5 mm were used owing to their similar behavior in terms of back pressure as washcoat on a monolith carrier at high space velocities of 90,000 h^{-1}.

Temperature dependent NO_X storage capacity measurements were also performed on the granules of a fully formulated LNT catalyst from a C segment vehicle as a reference to evaluate the contribution of each investigated material on the NSC and to identify possible synergistic effects of material combinations. The washcoat composition of the reference LNT was analyzed by inductively coupled plasma optical emission spectrometry (ICP-OES) and listed as specific loading (g/l_{cat}) and mass fraction (%) of each compound in Table 1. The reference LNT contains ceria (CeO_2) and aluminum oxides (Al_2O_3) with the highest mass fraction. The ceria takes over the functionalities for the medium temperature NO_X storage as well as oxygen storage functions. The Al_2O_3 is the main carrier for the PGMs, in this case Pt and Pd. Small amounts of rhodium were also found with a typical concentration of about 5 wt.-% of the Pt/Pd fraction. $MgAl_2O_4$ can also be seen as the low temperature NO_X storage material. As the most important NO_X storage material for a wider temperature range, BaO can be found in the catalyst composition. A detailed characterization of this catalyst has already been published in [8].

Table 1. Washcoat composition of the LNT reference.

Component	Pt	Pd	Rh	$MgAl_2O_4$	CeO_2	BaO	Al_2O_3
Specific Loading/(g/l_{CAT})	2.52	0.8	0.09	22.2	132	10	80
Mass Fraction/%	1.01	0.32	0.04	8.87	52.71	5.11	31.95

Given this analysis and the literature review, single catalysts are firstly synthesized for the investigations. Besides platinum-loaded $MgAl_2O_4$, ceria and 20 wt.-% BaO/Al_2O_3 as well-known NO_X storage materials, Pt on Al_2O_3 was also prepared to understand the NO_X storage behavior of the single support material. Physical mixtures of 50% Pt on Al_2O_3 and 50% CeO_2 with and without Platinum are fabricated due to their promising NO_X storage capacity at medium temperatures. Further. different combinations of single materials,

e.g., 50% $Pt/Ba_{20}/Al_2O_3$ + 50% Pt/CeO_2 and 50% $Pt/Ba_{20}/Al_2O_3$+ 50% $Pt/MgAl_2O_4$, were produced to investigate possible synergistic effects between the individual material types.

In addition, a Pt loaded $Ba_{10}Ce_{25}/Al_2O_3$ infiltration composite was synthesized by double IWI impregnation of alumina with 25 wt.-% CeO_2 and 10 wt.-% of BaO, due to its excellent NO_X storage performance based on the low diffusion distance for NO_X between the functional materials compared to physical mixtures of these components [37]. Moreover, the platinized infiltration composite was coated with Rh to observe the influence of Rh under lean conditions. The investigated NO_X storage materials and their combinations are summarized in Table 2.

Table 2. Investigated NO_X storage materials.

Samples	Material
Reference LNT	From serial production
Pt/Al_2O_3	Commercial alumina
$Pt/MgAl_2O_4$	Commercial Mg spinel
50% Pt/Al_2O_3 + 50% CeO_2	Non-activated commercial ceria
50% Pt/Al_2O_3 + 50% Pt/CeO_2	Activated commercial ceria
$Pt/Ba_{20}/Al_2O_3$	Activated barium (Infiltration composite)
50% $Pt/Ba_{20}/Al_2O_3$ + 50% Pt/CeO_2	Mixture of ceria and barium
50% $Pt/Ba_{20}/Al_2O_3$ + 50% $Pt/MgAl_2O_4$	Mixture of Mg spinel and barium
$Pt/Ba_{10}Ce_{25}/Al_2O_3$	Infiltration composite
$Pt/Rh/Ba_{10}Ce_{25}/Al_2O_3$	Infiltration composite

First, the temperature dependent NO_X storage capacities of the individual washcoat components and a mixture of 50% Pt/Al_2O_3 + 50% Pt/CeO_2 in comparison to the reference LNT were investigated (Figure 1). As expected, the fully formulated LNT has the maximum NSC of 162 µmol/g_{Cat} at $T_{inlet} = 250$ °C which corresponds to a storage capacity of around 2 g NO_2 equivalent with a normal washcoat loading of 250 g/L on the monolith at this temperature. As the basic washcoat support material platinized alumina (Pt/Al_2O_3) has a considerable NSC at temperatures below $T_{inlet} = 300$ °C, which supports the findings of Sedlmair et al. [38] and Epling et al. [10]. A replacement of 50% of the alumina with the bulk of Pt coated ceria (50% Pt/Al_2O_3 + 50% Pt/CeO_2) does not have a remarkable impact on the NO_X storage performance compared to NSC of the individual alumina over the complete temperature range. A lower NO_X storage capacity at temperatures below $T_{inlet} = 300$ °C can be detected with Pt doped barium oxides ($Pt/Ba_{20}/Al_2O_3$) in comparison to the single aluminum oxides (Pt/Al_2O_3). It was already indicated by Olsson et al. [15] that much more platinum oxides are formed on $Pt/Ba_{20}/Al_2O_3$ than Pt/Al_2O_3, which leads to a negative effect on NO oxidation at low temperatures, because the formation and stability of the less reactive Pt oxides blocks the active Pt sites and reduces the exposed surface area of metallic Pt and other PGMs. Therefore, NO_2 formation and thus NO_X adsorption over the nitrate route on barium slows down and results in a lower NO_X storage capacity at low temperatures. At higher temperatures, the stability of the platinum oxide decreases, leading to an enhanced exchange rate of the gas species involved on the platinum surface and thus increasing the NO oxidation performance. At high temperatures, such $T_{inlet} = 350$ °C and $T_{inlet} = 450$ °C. However, the NO_X storage level of the individual barium oxides is even higher than that of the optimized reference LNT. Comparable NO_X storage to the reference is achieved with the platinized Mg spinel at $T_{inlet} = 150$ °C. Apparently, the same kinetic limitation of NO oxidation activity on the Pt sites, found for the $Pt/Ba_{20}/Al_2O_3$ catalyst at these low temperatures, was also dominant for the platinized Mg spinel system. With increasing temperature, the $MgAl_2O_4$ can store slightly more NO_X. Nonetheless, it is not at the level of the Ba-containing materials or the reference LNT.

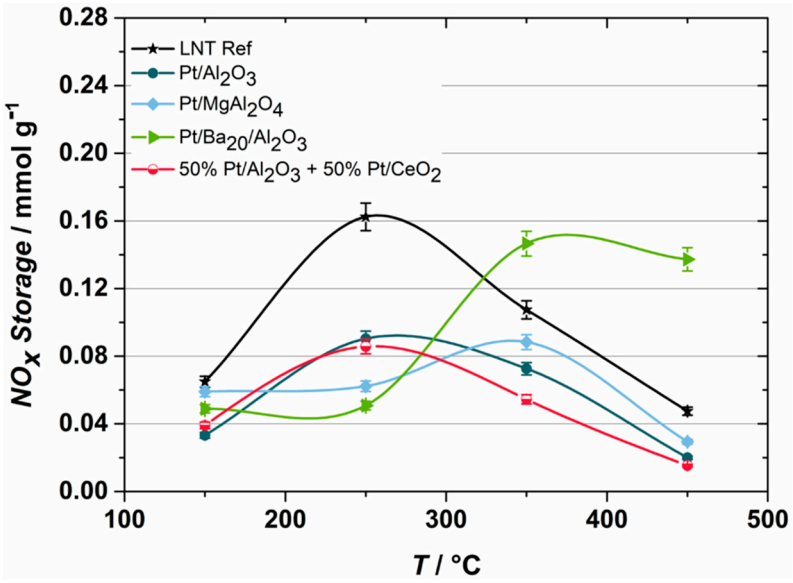

Figure 1. Temperature-dependent NO_X storage capacity of individual materials and material combinations compared to the fully formulated reference LNT.

To determine the effect of the Pt loading on ceria in particular, NSC measurements were also performed on a non-activated CeO_2 in the mixture of 50% Pt/Al_2O_3 + 50% CeO_2, which was compared in Figure 2 with the Pt-activated ceria-based substance (50% Pt/Al_2O_3 + 50% Pt/CeO_2). Both systems reached the maximum NO_X storage capacity at $T_{inlet} = 250$ °C. However, the Pt activation significantly shifts the NSC in the medium temperature range up to 20% at $T_{inlet} = 250$ °C and 30% at $T_{inlet} = 350$ °C. This exhibits the influence of the Pt sites on ceria surface on the NO_X storage performance, especially in the medium temperature range.

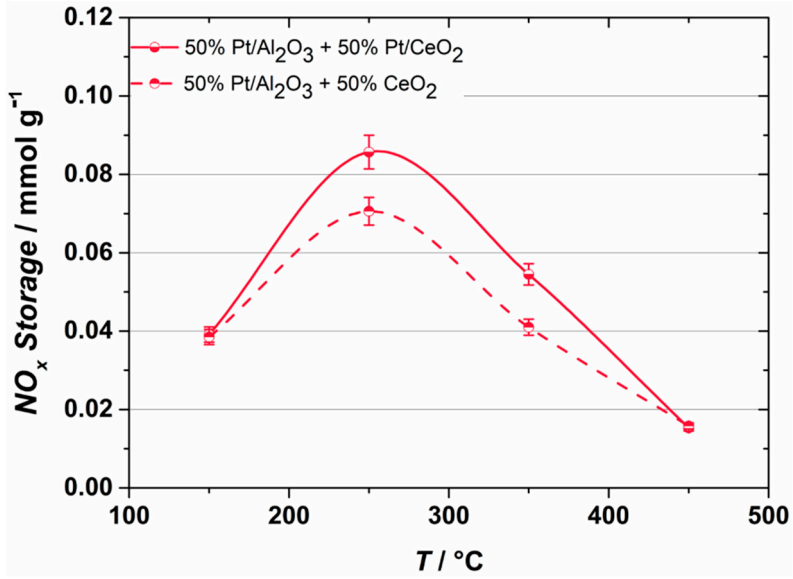

Figure 2. Temperature dependent NO_X storage capacity from non-activated ceria (black line) and platinized CeO_2 (dashed line) in a physical mixture with Pt/Al_2O_3.

Another batch of physical mixtures of the individual catalysts were investigated under same boundary conditions in order to find synergistic effects. Figure 3 shows the NO_X storage capacities of a mixture of 50% Mg spinel and 50% BaO (50% $Pt/MgAl_2O_4$ + 50% $Pt/Ba_{20}/Al_2O_3$) (see Figure 3a) as well as a mixture of 50% ceria and 50% BaO

(50% Pt/CeO_2 + 50% $Pt/Ba_{20}/Al_2O_3$) (see Figure 3b) compared to their single compounds. In addition, a calculated value of the expected NO_X storage capacity regarding to their mixture composition is plotted for both diagrams in Figure 3. The expected NSCs were determined via Equation (1), where $n_{NOx,i}$ indicates the NO_X storage capacity of the individual materials, and φ_i gives the volume fraction of each material in the physical mixture at certain temperatures.

$$n_{NOx,mix} = \sum \varphi_i n_{NOx,i} \quad (1)$$

At high temperatures, an enhanced NO_X storage was obtained with the mixture of barium oxide and Mg compared with the individual materials and the expected calculated NSC. Apparently, a synergistic effect is responsible for observed higher NO_X storage performance at $T_{inlet} = 350$ °C. Furthermore, the combinatorial approach to the development of a substance used in these investigation results is an improvement over the fully formulated LNT reference (see Figure 1). Since BaO sites adsorb NO_2 more efficiently than NO [12,13], the Mg spinel phase in the mixture can be expected to increase the formation of NO_2 from the supplied NO and O_2, which can be easily captured by barium oxide. Accordingly, Mg spinel prepares a suitable environment for enhanced NO_X storage at elevated temperatures.

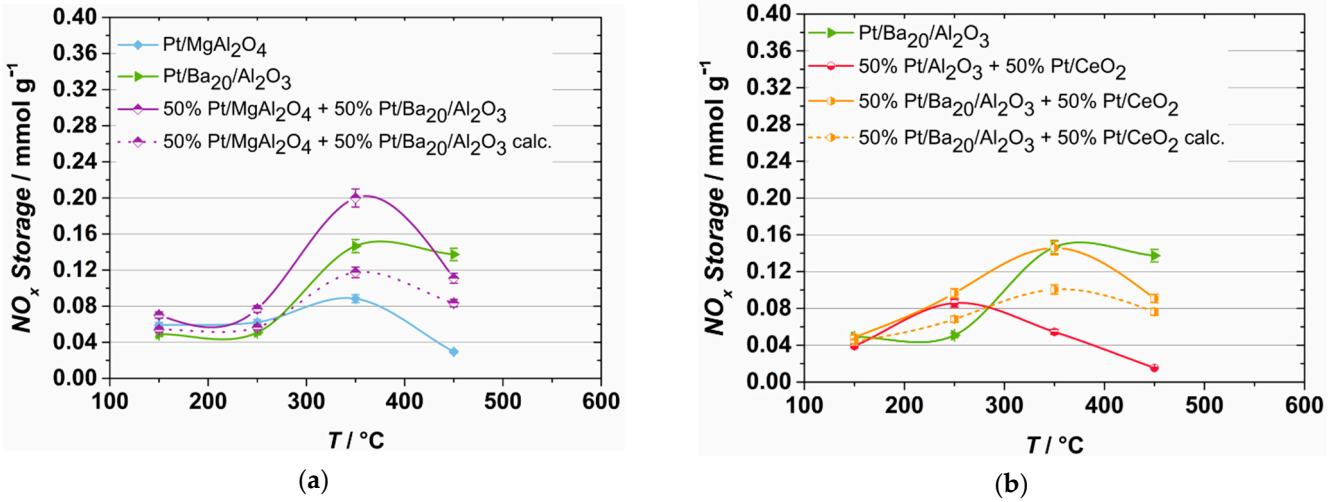

(**a**) (**b**)

Figure 3. Maximum NO_X storage capacity of Mg spinel and BaO as well as their physical mixture (**a**) and that of ceria and BaO with their physical mixture (**b**) in comparison to the expected NO_X storage performance of the mixtures (dotted lines).

A similar observation can also be taken from the results of the physical mixture between ceria and BaO. A higher NO_X storage capacity at $T_{inlet} = 250$ °C compared to the calculations could be achieved as a result of the synergistic effect between both materials. This can also be explained by the promoting effect of ceria on the NO oxidation to NO_2. Since NO_2 formation reaches its maximum around $T_{inlet} = 350$ °C, no difference can be determined between the mixture and individual $Pt/BaO/Al_2O_3$ catalyst. In comparison to the mixture between Mg spinel and Ba_{20}/Al_2O_3, lower NO_X storage capacity was measured at high temperatures owing to the lack of adsorption sites present in the mixture.

Moreover, it is imperative to exploit the additional synergistic effects between the catalytic materials to achieve acceptable NO_X storage in the low and medium temperature range for automotive applications. The so far shown synergistic effects could significantly improve the NSC only above $T_{inlet} = 300$ °C. To enhance the NO_X adsorption capacity at $T_{inlet} = 250$ °C to the level of the reference material, PGM-loaded BaO and ceria containing infiltration composites (IC) ($Pt/Ba_{10}Ce_{25}/Al_2O_3$ and $Pt/Rh/Ba_{10}Ce_{25}/Al_2O_3$) were synthesized by impregnating PGM, BaO, and ceria in the pore system of an alumina support to reduce the diffusion pathways of NO_X molecules.

The obtained NO_X storage capacities over the temperature of these compounds are plotted in Figure 4 and compared to the material mixtures from Figure 3 and the reference LNT. Low NSCs be found at the temperature around T_{inlet} = 150 °C for all investigated materials. At T_{inlet} = 350 °C and above all synthetized mixtures within this work can achieve a much higher NO_X storage capacity compared to the LNT reference. The mixture of Mg spinel and BaO exhibits a considerably higher NSC at T_{inlet} = 350 °C and exceeds the maximum NO_X storage of the reference material and the expectations from the performance of their components.

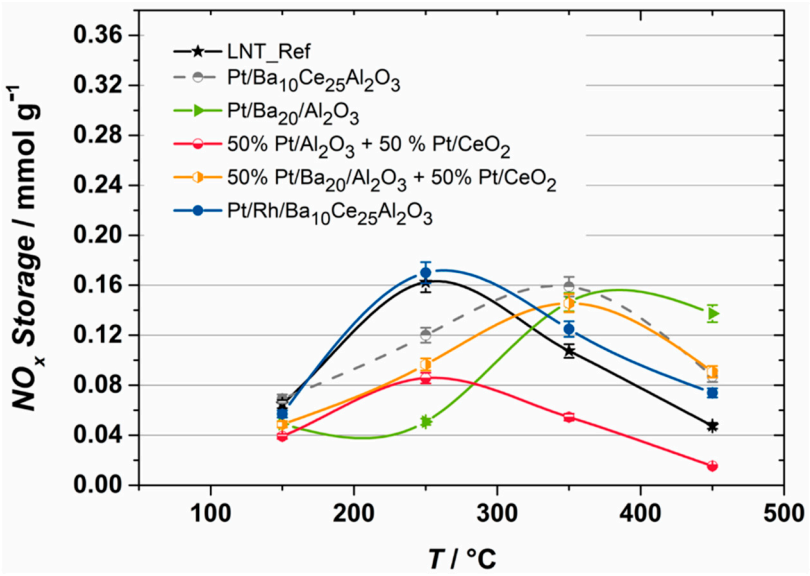

Figure 4. Temperature-dependent NO_X storage capacity of different physical catalyst mixtures, different PGM loaded infiltrations composites and the reference LNT.

A remarkable observation can be taken from the investigations on IC material with different PGM loadings. At T_{inlet} = 250 °C, the IC material $Pt/Ba_{10}Ce_{25}/Al_2O_3$ without Rh cannot reach the NO_X storage level of the reference LNT, but exhibits a better performance at T_{inlet} = 350 °C and above. However, the additional Rh loaded IC material $Pt/Rh/Ba_{10}Ce_{25}/Al_2O_3$ features a comparable performance as the reference LNT at T_{inlet} = 250 °C as well as a better performance at T_{inlet} = 350 °C. Both IC materials can achieve higher NO_X storage levels than the physical blends of the corresponding single materials at T_{inlet} = 250 °C. The proximity of the BaO sites with the Pt sites and their dispersion on the surface in the IC materials ensure a higher NO_X storage performance. The Rh variation reveals another function of Rh on an LNT. The NSC of the IC material $Pt/Rh/Ba_{10}Ce_{25}/Al_2O_3$ is promoted by the Rh in particular at lower temperatures around T_{inlet} = 250 °C. It can be observed that Rh, which is usually applied to enhance the NO_X regeneration performance during rich phases, shows also a NO_X storage activating effect during lean phases. In this case, a low amount of Rh causes an improvement of 45% in the NO_X storage capacity at this temperature.

2.2. Oxygen Storage Capacity

Another crucial aspect of modern LNTs is their oxygen storage capacity (OSC), which is mainly provided by the platinized ceria component in the washcoat. This can significantly influence the regeneration behavior by additionally oxidizing the reductants during the initial phase at the beginning of rich conditions, thus leading to a less efficient and extended NO_X regeneration [8]. For this reason, OSC of the ceria containing catalysts and of the reference LNT are evaluated at various temperatures. The results of these OSC measurements are shown in Figure 5.

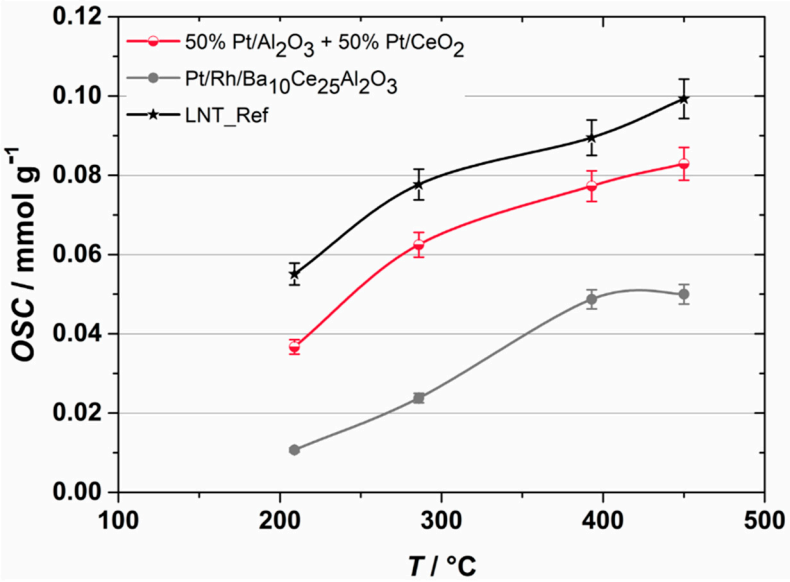

Figure 5. Temperature dependent oxygen storage capacities the reference LNT and the different Ceria containing catalysts.

In general, the oxygen storage of the individual material increases with increasing temperature. Due to the high ceria amount (approx. 108 g/L_{Cat}) of the reference LNT, a high OSC is determined for the entire temperature range, which is increased from 55.1 µmol/g_{Cat} to 88.3 µmol/g_{Cat} at T_{inlet} = 200 °C and T_{inlet} = 450 °C respectively. A comparable OSC can be achieved with the physical mixture of 50% Pt/Al_2O_3 + 50% Pt/CeO_2. The maximum OSC of this catalyst reaches 82.9 µmol/g_{Cat} at T_{inlet} = 450 °C. The reduced ceria amount (approx. 40.7 g/L) allows the IC material $Pt/Rh/Ba_{10}Ce_{25}Al_2O_3$ to reduce the OSC of 50% at T_{inlet} = 450 °C.

3. Discussion

Various platinized commercial NO_X storage materials representing the washcoat composition of state-of-the-art LNTs, and physical mixtures of them were analyzed under realistic test conditions in terms of their NSC and OSC to quantify possible synergistic effects and to track the storage performance of a fully formulated commercial LNT. It was found that the obtained NSC of the individual catalytic materials Pt/Al_2O_3, Pt/CeO_2 $Pt/Ba_{20}/Al_2O_3$, and $Pt/MgAl_2O_4$ could not explain the storage behavior of such LNTs. Some significant improvements in NSC could be achieved by a combinatorial approach of the different catalyst types, especially by coating the ceria with platinum, but the important gap in maximum NO_X storage performance at T_{inlet} = 250 °C cannot be reproduced with the physical mixtures of the individual materials.

Interestingly, the combination of Pt/Mg-spinel and $Pt/Ba_{20}/Al_2O_3$ shows a remarkable increase in the NSC at temperatures above T_{inlet} = 300 °C, which was around 50% higher than the expected value which was calculated from the performance of each individual catalyst. In principle, the same behavior was observed for the mixture of Pt/CeO_2 and $Pt/Ba_{20}/Al_2O_3$, but only a small increase in the NSC at T_{inlet} = 250 °C could be achieved. This was unexpected, since platinized ceria have a superior oxidation capability to convert NO to NO_2 at low and medium temperatures and can store NO_X in the same temperature region [21]. Consequently, the maximum NO_X storage capacity normally shifted to lower temperatures of about 250 °C. Obviously, the ceria used was not able to support this function. To overcome this limitation and to advance the washcoat technology of LNTs, PGM- loaded infiltration composites were developed based on ceria and barium oxide coatings within pore system of an alumina support. This was first introduced by Shi et al. [37] as an excellent storage material for medium temperatures.

To illustrate the effect of this measure, the textures of both catalysts are shown schematically in Figure 6. The washcoat of the reference LNT (see Figure 6a) consists of a physical mixture of PGM-loaded alumina (light grey) and ceria (orange) phases with grain sizes between 2 to 5 µm. The BaO phase (green) with a comparable grain size is randomly distributed within this matrix. According to this texture, long diffusion pathways of the NO_2 molecules must be bridged from the active precious metal centers to the storage sites of the support materials (e.g., from Pt to BaO).

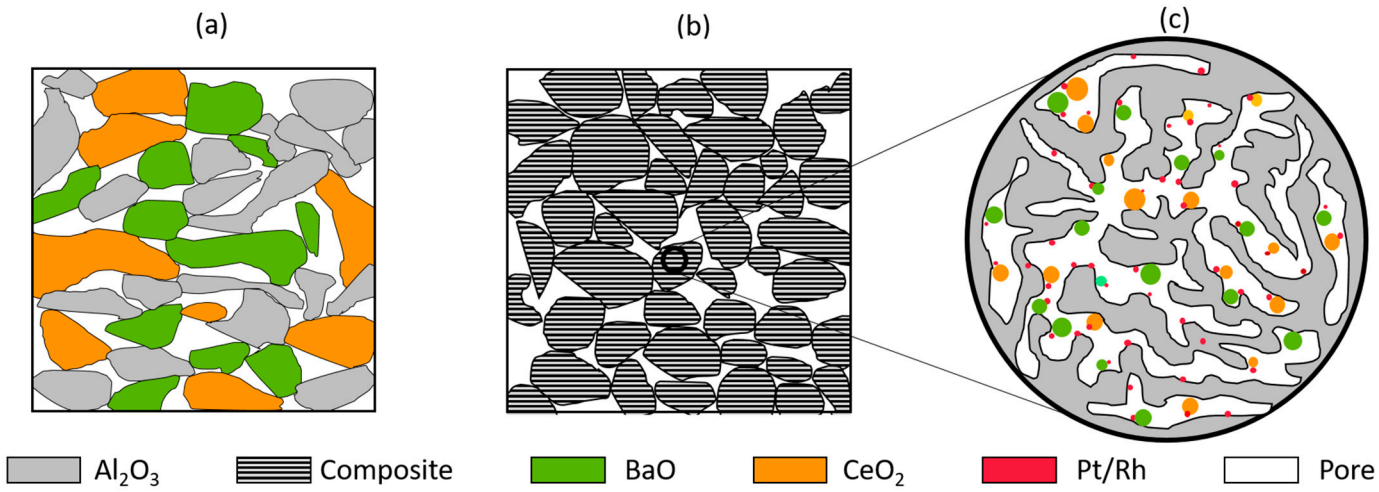

Figure 6. Textures of (**a**) the reference LNT, (**b**) the infiltration composite ($Pt/Rh/Ba_{10}Ce_{25}Al_2O_3$) and (**c**) the distribution of the functional materials within the pore system of the alumina support (zoom).

In contrast to the reference LNT, the catalyst texture of the infiltration composite $Pt/Rh/Ba_{10}Ce_{25}Al_2O_3$ macroscopically consists of only this one material (see Figure 6b), where the PGM, ceria and barium oxide were coated as nanoparticles in the inner pore structure of the Al_2O_3 base support, as illustrated in Figure 6c. This provides an excellent dispersion of active materials, which significantly reduces the diffusion pathways for complex reactions of all participants. Obviously, this proximity of the components enables a higher production of storable NO_X species on the active surface and their subsequent storage on the nearby Ba sites. As a consequence, a slightly higher molar NO_X storage level above 250 °C can be achieved with the single platinized IC material compared to the mixture of $Pt/MgAl_2O_4$ and $Pt/Ba_{20}/Al_2O_3$. Surprisingly, with the addition of small amounts of Rhodium to the platinized IC material, the maximum NSC shifted to 250 °C, resulting in a comparable storage performance to the reference LNT. The reason for this enormous synergistic effect is not understood at the moment and may be related to favorable distribution of the Rhodium on the directly adjacent active materials within the composite. This is a subject of further investigations. However, this result highlights the important contribution of this precious metal to the overall performance of LNTs and not only to regeneration.

Furthermore, the results of the OSC measurements indicate that the reference LNT can store about 50% more oxygen at all temperatures studied. However, a high OSC is not favored for a good NO_X regeneration because the oxidation of the reductants during rich phases with the stored oxygen at the surface leads to an unnecessarily high consumption of the reductants, thus prolonging the NO_X regeneration. Therefore, the regeneration efficiency can also be enhanced based on the lower OSC of the IC material $Pt/Rh/Ba_{10}Ce_{25}/Al_2O_3$.

4. Materials and Methods

4.1. Catalyst Preparation

A series of platinum containing catalysts on different commercial supports were prepared. First, Al_2O_3 (Puralox TH 100/150, Sasol Germany), $MgAl_2O_4$ (Puralox Mg26, Sasol

Germany), the infiltration composites (IC) of 20% BaO/Al_2O_3 (abbreviated as $Ba_{20}Al_2O_3$) and 10% $BaO/25\%$ CeO_2/Al_2O_3 (abbreviated as $Ba_{10}Ce_{25}Al_2O_3$) were coated with 2.5 wt.-% of platinum via incipient wetness impregnation (IWI). For this purpose, 1.23 g $H_2Pt(OH)_6$ (ABCR, Karlsruhe Germany) and 1.5 g $(CH_3)_4NOH\bullet 5\ H_2O$ (Alfa Aesar, Germany) were dissolved in 27 to 45 mL of water and mixed with 27.5 g of the respective powder. For the CeO_2 (Interkat, Königswinter, Germany) with a commercial Pt-loading of 1 wt.-%, only 0.475 g of the Pt precursor and 0.579 g of the tetramethylammonium hydroxide were dissolved in 21 mL of water and mixed with 29.7 g of the powder. The corresponding volumes for the solutions used were adjusted in advance to match the water adsorption capacity of each powder. Subsequently, the wet powders were dried at 140 °C and calcined for 1 h at 550 °C with a heating rate of 175 °C/h.

The additional Rhodium coating of the platinized $Ba_{10}Ce_{25}Al_2O_3$ catalyst with a Rh content of 0.125 wt.-% (5 wt.-% of the Pt amount) was carried out in an analogous way by infiltration of 30 g of the composite with a solution of 0.104 g $Rh(NO_3)_3$ hydrate (36 wt.-% Rh content, Merck, Darmstadt, Germany) in 28 mL water, followed by the same heat treatment used for the Platinum coating.

The IWI method was also used for the preparation of the infiltration composites. For the syntheses of 27.5 g of the 20 wt.-% BaO/Al_2O_3 composite, 9.16 g $Ba(CH_3COO)_2$ (Merck, $\geq$99.0%, Germany) was dissolved in 41 mL distilled water and infiltrated onto 22 g of commercial Al_2O_3, (Puralox TH 100/150, Sasol Germany). After drying at 140 °C (5 h), the material was calcined for 1 h at 550 °C with a heating rate of 175 °C/h.

The 10% $BaO/25\%$ CeO_2/Al_2O_3 composite was prepared in two steps. First 25 wt.-% Ceria was loaded on commercial alumina (Puralox TH 100/150, Sasol Germany) followed by an additional BaO coating of 10 wt.-% after a subsequent drying and calcination step. For the syntheses of 27.5 g of this infiltration composite, 17.87 g of the alumina was primarily mixed with a solution of 17.34 g $Ce(NO_3)_3\bullet 6\ H_2O$ in 29 mL water. The wet powder was dried at 140 °C and calcined at 550 °C (heating rate: 175 °C/h). Next, the Ceria impregnated powder was mixed with 24 mL of an aqueous solution containing 4.58 g $Ba(CH_3COO)_2$, followed by the same heat treatment used in the first coating step.

4.1.1. Granule Formation

To avoid pressure-drop during performance tests, the reference LNT, the single catalyst powders, or the physical mixtures of them and the composites, were first milled to an average grain size of 2–3 µm (D_{50}) and processed into granules. Therefore, 200 mL of distilled water was added to 60 g of each catalyst powder to form slurries, which then were milled for 2 h on a roller bench with 1 kg of 5 mm ZrO_2 balls. The grain size distribution was controlled using laser diffraction measurements (Malvern Mastersizer Microplus, United Kingdom). Subsequently, the slurries obtained were separated from the milling balls, dried at 140 °C and ground to powder.

For granule formation, 20 g of each powder was mixed with 2.5 g AlO(OH) sol (solid fraction 24%), 0.6 g ethylene glycol (Merck), 0.3 g Optapix® (polyvinyl alcohol compound, Zschimmer & Schwartz) and water until a homogenous paste was obtained. The creamy mass was applied in thin stripes on a plate using a syringe. After drying (140 °C, 2 h), the stripes were cut down into small granules and sieved to a grain size fraction of 1 to 1.5 mm. Finally, the granules were calcined by heating up in air at a rate of 175 °C/h to 550 °C for 1 h.

The AlO(OH) sol used was prepared by mixing 45 g of boehmite powder (Disperal, Sasol, Germany) with 96 mL of water and 9 mL of 2 M nitric acid. The resulting suspension was dispersed at 8000 rpm by an Ultra turrax. After a few days of rest at room temperature under ambient conditions, a viscous gel was obtained before use. The complete process for preparing the catalyst samples is summarized in the flow chart in Figure 7.

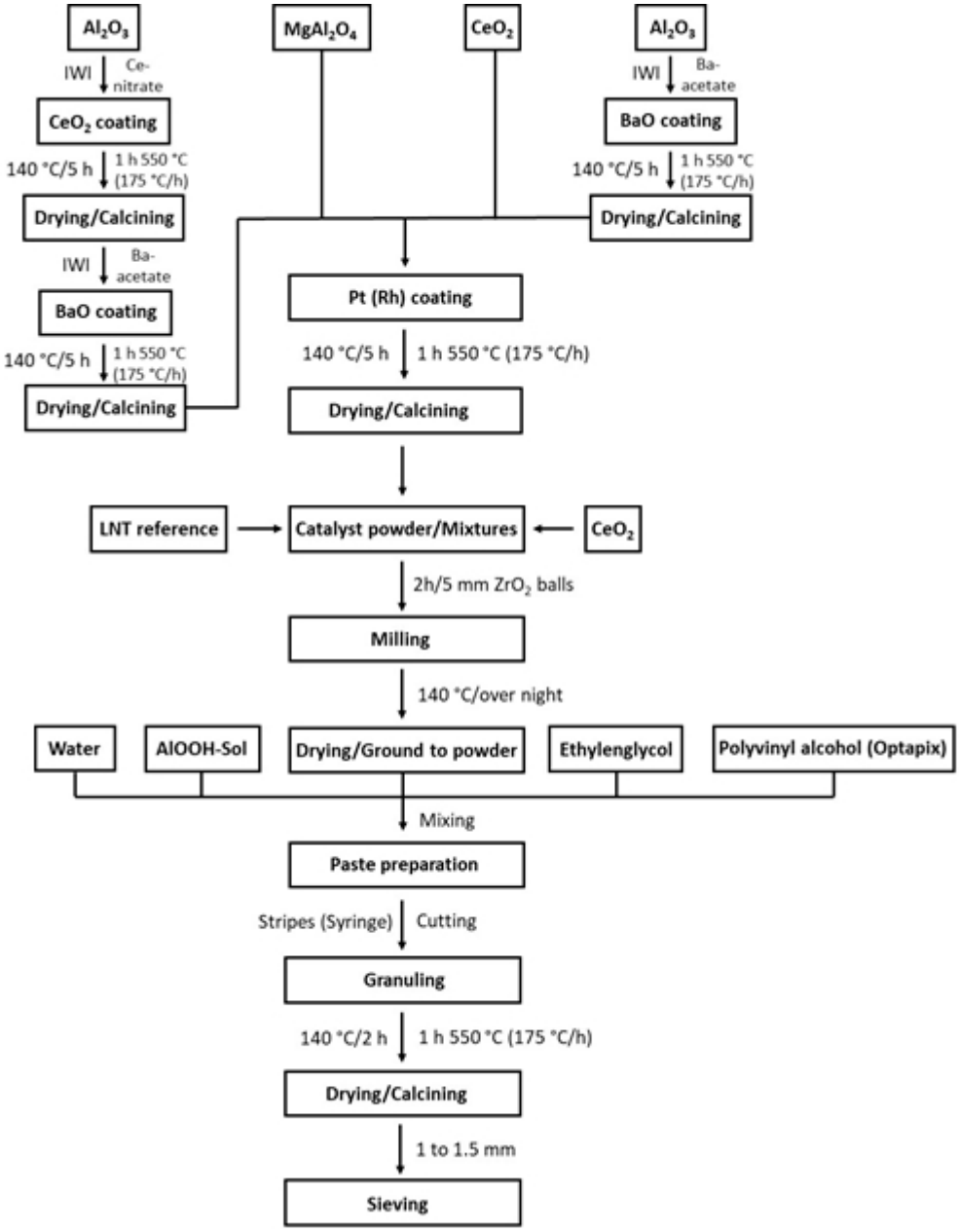

Figure 7. Flow chart of the catalyst.

4.1.2. Grain Size Distribution

To guarantee a comparable grain size distribution between 2 and 3 µm of the catalyst powders before granulizing, laser diffraction measurements were carried out by using a Mastersizer Microplus MAF 5001 (Malvern Panalytical,UK). Therefore, a few drops of each slurry were dispersed by supersonic in 500 mL of a solution with 1 wt.-% $Na_4P_2O_7 \times 10\ H_2O$ (dispersant) in water and pumped though the measurement cell. For analysing, the angular variation in intensity of light scattered as a laser beam (He-Ne laser, 633 nm) passes through a dispersed particulate sample was measured. The grain size distribution was calculated from the obtained intensity data by Mastersizer Microplus software, version 2.18 using Mie theory of light scattering and the Fraunhofer approximation.

4.2. Reference Catalyst

As reference, a commercial LNT was obtained from a serial production vehicle with a 1968 cm^3 diesel engine (68.6 kW/l nominal specific power) based on a metal foil mono-

lith with a diameter of 11.5 cm and length of 13.8 cm (V_{LNT} = 1433 cm^3). To obtain an undamaged sample, the entire LNT was first embedded in pure ash-free hard wax before sawing. Then, a rectangular slice of about 50 mL was cut out and de-waxed by Soxhlet extraction with hexane followed by calcination at 600 °C for 5 h in air. Subsequently, the complete washcoat was detached from the metal foil, ground into a powder and processed into granules (see Section 4.1.1).

4.3. Experimental Setup

In order to investigate the NO_X and oxygen storage behavior of the different catalytic materials under defined boundary conditions, a laboratory gas test bench (LGB) was used. The schematic of the LGB is shown in Figure 8. The test bench mainly consists of a reactor part, in which the sample, flow controller, heater, and valves are installed, a LabVIEW-based control and regulation unit, and the measurement technology. The capabilities of the test bench have already been published elsewhere [8,39–42].

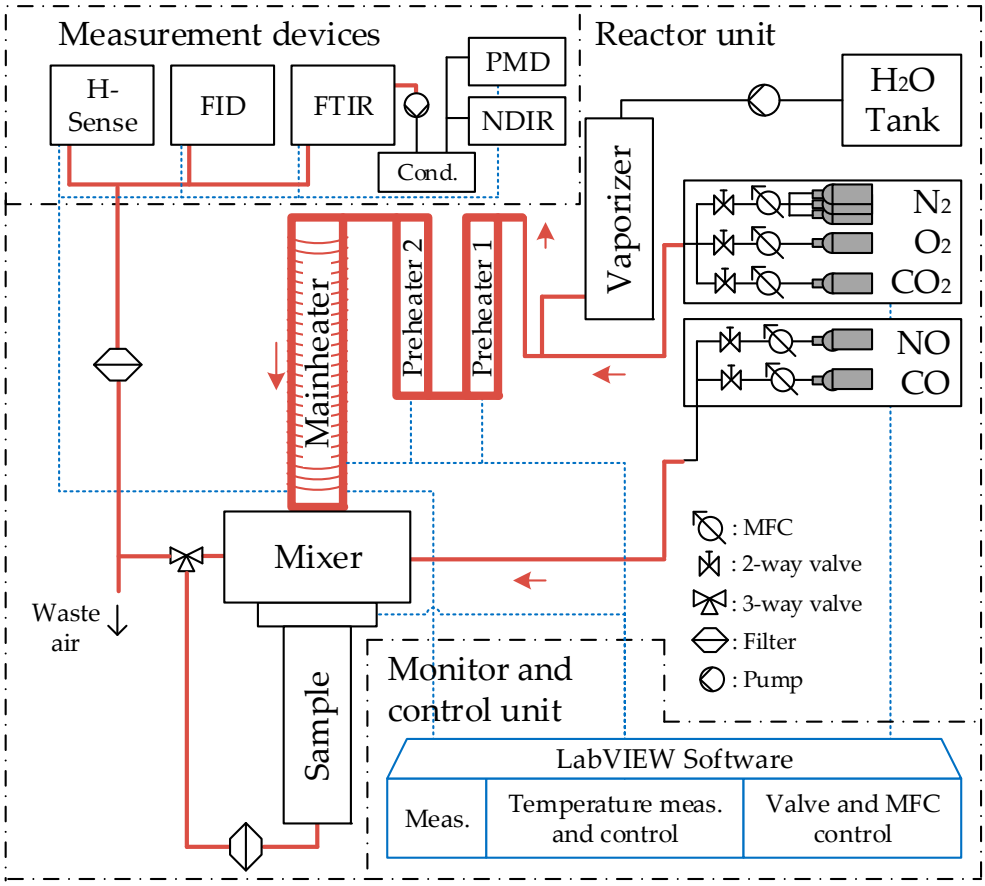

Figure 8. Schematic of the laboratory gas test bench.

The feed gas stream can be supplied in the desired concentrations through the specified titanium pipes, which are heated to 190 °C as standard. The volume flow rates for the individual test gases are dosed from gas bottles with mass flow controllers (MFCs) of the type SLA5850 from Brooks Instrument, LLC (Hatfield, PA, USA). This allowed to regulate the targeted space velocity and the gas concentrations for the individual experiments. The gas bottles with nitrogen and oxygen usually contain pure gases, while the concentrations for the other components are between 0.9 and 2% in nitrogen. The water required for the tests was provided via a separated water vaporizing system.

The temperature of the flowing gas, as well as the temperature through the length of the catalyst sample are regulated by a two-stage heating system. The modeled exhaust gas mixture of the high concentration gases such as N_2, O_2, CO_2 and H_2O are first heated

by two preheaters in a separate line and then a main heater. This provides most of the required power to heat the gas mixture. The preheaters and the main heater are controlled via closed loop control during tests. To achieve a homogeneous change in temperature across the entire test bench, i.e., to enable a temperature ramp, the temperature set points of the entire heating system are coupled with the set points of the preheaters and the main heater. The lower-concentration feed gas components are mixed into the main gas mixture in a heated mixer upstream of the catalyst sample.

Various measuring instruments are used to determine the concentrations of different gas species. After filtering, the entire gas flows through a Fourier transform infrared spectrometer (FTIR) MultiGas 2030 from MKS Instruments, Inc. (Andover, MA, USA) to analyze H_2O, CO, CO_2, NO, NO_2, N_2O, and NH_3 concentrations with high accuracy. All measurement data were evaluated with a frequency of 1 Hz. A picture of the LGB with the main components and the sample is shown in Figure 9. The measurement devices are positioned on the other side of the test bench.

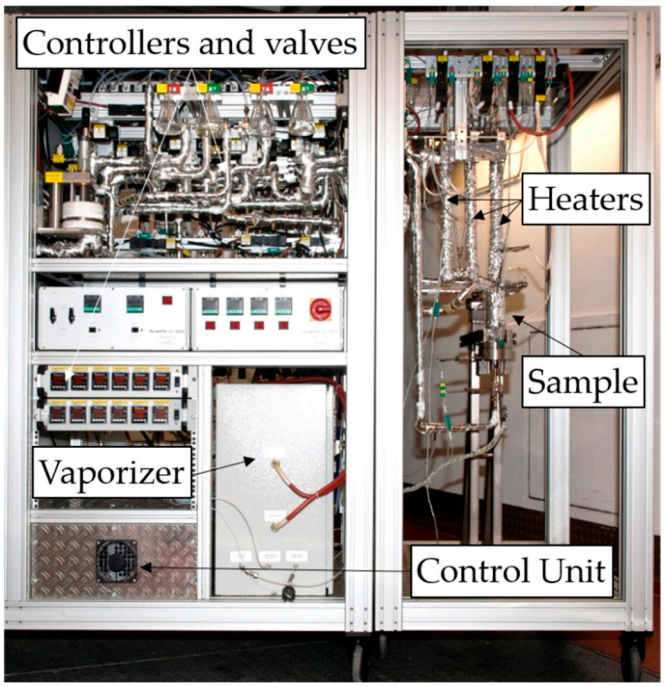

Figure 9. Picture of the laboratory gas test bench.

4.4. NO_X Storage Measurements

To compare the performance of synthetized catalysts with the reference LNT, the NO_X storage capacities are measured under realistic gas composition and space velocity in a temperature range between 150 °C and 450 °C derived from benchmark engine data. The boundary conditions are listed in Table 3.

Table 3. Conditions for NO_X storage capacity measurements.

Parameter	Value
Temperature/°C	150, 250, 350, 450
SV/1/h	90,000
NO/ppm	500
O_2/%	9
CO_2/%	6
H_2O/%	6
N_2/%	balance

To investigate NO_X adsorption behavior, all granules are hydrothermally pre-aged in air at $T = 750$ °C for 10 h with $\psi_{H_2O} = 10$ % water content. After de-greening, the granules are conditioned at $T = 110$ °C for 6 h and weighted prior to use. Before and after each measurement, the granules are conditioned at $T_{inlet} = 450$ °C with $\psi_{CO} = 700\ ppm$ in balance N_2 to ensure that NO_X adsorption sites are regenerated before the next measurement.

This preconditioning phase is followed by cooling with oxygen to the respective measurement temperature to achieve realistic conditions as in the vehicle. The NO_X storage capacities are measured at different temperatures between $T_{inlet} = 150$ °C and $T_{inlet} = 450$ °C. During NO_X storage measurements at four different temperatures of 150 °C, 250 °C, 350 °C, and 450 °C, the catalytic materials are treated with the feed gas until the dosed NO value was reached downstream of the samples. Then, the feed gas composition is changed to an inert mixture with nitrogen to remove the stored NO_X. Afterwards, the stored NO_X is desorbed by heating up the sample 450 °C. A subsequent post-conditioning is conducted with CO at the same temperature for a complete purging of the NO_X storage.

Finally, the specific molar NO_X adsorption $n_{NOx,ads,i}$ on the granules is calculated according to Equation (2), by integration of the difference between the NO_X molar flux upstream and downstream of the granules, i.e., $\dot{n}_{NOx,us}$ and $\dot{n}_{NOx,ds}$, from the beginning until to the end of dosing t_{end}. To have a specific NO_X storage value for each material, the integral is divided by the mass of the measured granules m_i.

$$n_{NOx,ads,i} = \frac{1}{m_i} \int_{o}^{t_{end}} \left(\dot{n}_{NOx,us} - \dot{n}_{NOx,ds}\right) dt \tag{2}$$

$$n_{NOx,des,i} = \frac{1}{m_i} \int_{t_{ramp\ start}}^{t_{ramp\ end}} \dot{n}_{NOx,ds} dt \tag{3}$$

The plausibility of the NO_X storage measurement is checked by comparison between integrals of the adsorbed NO_X on the catalyst and the desorbed NO_X value $n_{NOx,des,i}$ downstream the catalyst from the beginning ($t_{ramp\ start}$) to the end ($t_{ramp\ end}$) of the temperature ramp, as displayed in Equation (3). The deviations limits in measurements are plotted in all diagrams.

4.5. Oxygen Storage Capacity Measurements

The oxygen storage capacity (OSC) is a further important criterion for the evaluation of NO_X adsorbing materials. OSC studies are carried out at a constant inlet temperature with a cycling between two gas mixtures containing either 2% CO or 1% O_2 and N_2 as carrier gas. The boundary conditions for OSC measurements are listed in Table 4. Water is not included in the gas mixture to prevent side reactions such as water gas shift reaction with the dosed CO. After conditioning at $T_{inlet} = 450$ °C with $\psi_{CO} = 700\ ppm$ and cooling to the respective measurement temperature, O_2 is first added primarily to fulfill O_2 storage.

Table 4. Conditions for oxygen storage measurements.

Parameter	Lean	Rich
Temperature/°C	200, 300, 400, 450	200, 300, 400, 450
SV/1/h	90,000	90,000
CO/%	0	2
O_2/%	1	0
N_2/%	balance	balance

After reaching the dosing concentration, a short purging with inert mixture is conducted. This is followed by CO dosing to remove stored oxygen into CO_2. This cycle is repeated ten times to create a reproducible storage and reduction behavior.

The oxygen storage is calculated from CO_2 production during the CO dosing phases, as expressed in Equation (4), where the molar flow of the produced CO_2 $\dot{n}_{CO_2,produced}$ during rich phases is integrated between the start time of the CO dosing $t_{COdos,start}$ and the end time of the CO_2 peak $t_{CO_2peak,end}$ after switching to the rich phase. Since CO reacts with an O atom from the OSC ($CO + \frac{1}{2}O_2 \rightarrow CO_2$), molar flux for CO_2 is divided by 2 to achieve the actual oxygen storage.

The residual humidity on the catalyst surface can cause the water-gas shift reaction ($CO + H_2O \leftrightarrow CO_2 + H_2$) in the first cycles, which leads to a further consumption of dosed CO and an additional H_2 production. A correction of the molar H_2 flow $\dot{n}_{H_2,produced}$ is also implemented in the calculated value. The value after the first CO_2 peak at the turning point of each cycle is picked and the average of the last three cycles is used for ranking.

$$n_{O_2,i} = \frac{1}{m_i} \int_{t_{COdos,start}}^{t_{CO_2peak,end}} \left(\frac{1}{2} \dot{n}_{CO_2,produced} - \dot{n}_{H_2,produced} \right) dt \quad (4)$$

5. Conclusions

In this work, fundamental investigations of the NO_X and oxygen storage behavior on re-produced single washcoat components, identified by the analysis of a commercial LNT (reference LNT) and physical mixtures of them as well as PGM-loaded infiltration composites, are carried out in a laboratory test bench in granular form under realistic boundary conditions. The following conclusions can be drawn from the results:

- Due to synergistic effects, combination materials, in particular physical mixtures between Mg spinel and barium oxide or ceria and barium oxide, have been developed that can store more NO_X at higher temperatures than the commercially manufactured reference. As a result, modeling the combined performance by simply interpolating the NSC of the individual materials is not possible.
- The investigations with different material groups showed that a mixing process at the chemical level by impregnation of PGM, BaO, and ceria within the pore system on an alumina support is required to achieve a high NO_X adsorption capability at low temperatures by reducing the diffusion pathways for complex reactions of all participants.
- The variation of PGM within these infiltration components shows that only the addition of Rh could improve the NSC under lean conditions at $T_{inlet} = 250$ °C compared to the reference LNT.
- The oxygen storage capacity of the infiltration composites can be reduced by decreasing the amount of ceria without performance loss during NO_X storage, which could improve the NO_X regeneration efficiency.
- Due to the comparable NO_X storage performance with the reference LNT, the investigated $Pt/RhBa_{10}Ce_{25}Al_2O_3$ catalyst could be used as a single compound in commercial LNTs. However, further investigations and optimizations must still be executed in terms of regeneration behavior and HC oxidation activity (e.g., addition of Pd) to verify the suitability.

Author Contributions: The conceptualization and methodology were done by C.Ö., J.D. and P.M. All investigations were carried out by C.Ö. The project administration, funding acquisition and the necessary resources were provided by M.G. and S.P. Supervision was carried out by C.Ö., J.D., P.M., S.S., M.G. and S.P. The original draft was prepared by C.Ö., J.D., P.M., S.S. and M.G. S.P. contributed to the writing-review and editing process. All authors have read and agreed to the published version of the manuscript.

Funding: The EAGLE project has received funding from the European Union's Horizon 2020 research and innovation program [grant agreement No 724084].

Data Availability Statement: The data presented in this study are available on request from the corresponding author. The data are not publicly available due to the complexity of the analysis which needs guidance for reproduction.

Acknowledgments: The presented results were obtained within the EU-funded "EAGLE" project. The authors thank all participants of the project for the great cooperation during the entire project period. Furthermore, the authors thank all unnamed colleagues from TME for their contribution to the results.

Conflicts of Interest: The authors declare no conflict of interest.

References

1. Yang, L. NOx control technologies for Euro 6 diesel passenger cars: Market penetration and experimental performance assessment. *ICCT* **2015**. [CrossRef]
2. Johnson, T.V. Review of Vehicular Emissions Trends. *SAE Int. J. Engines* **2015**, *8*, 1152–1167. [CrossRef]
3. Nova, I.; Tronconi, E. *Urea-SCR Technology for deNOx after Treatment of Diesel Exhausts*; Springer: New York, NY, USA, 2014; ISBN 978-1-4899-8071-7.
4. Brandenberger, S.; Kröcher, O.; Tissler, A.; Althoff, R. The State of the Art in Selective Catalytic Reduction of NO x by Ammonia Using Metal-Exchanged Zeolite Catalysts. *Catal. Rev.* **2008**, *50*, 492–531. [CrossRef]
5. Miyoshi, N.; Matsumoto, S.; Katoh, K.; Tanaka, T.; Harada, J.; Takahashi, N.; Yokota, K.; Sugiura, M.; Kasahara, K. Development of New Concept Three-Way Catalyst for Automotive Lean-Burn Engines. In *SAE Technical Paper Series*; SAE International: Warrendale, PA, USA, 1995.
6. Liu, G.; Gao, P.-X. A review of NOx storage/reduction catalysts: Mechanism, materials and degradation studies. *Catal. Sci. Technol.* **2011**, *1*, 552. [CrossRef]
7. Roy, S.; Baiker, A. NOx storage-reduction catalysis: From mechanism and materials properties to storage-reduction performance. *Chem. Rev.* **2009**, *109*, 4054–4091. [CrossRef]
8. Schönebaum, S.; Dornseiffer, J.; Mauermann, P.; Wolkenar, B.; Sterlepper, S.; Wessel, E.; Iskandar, R.; Mayer, J.; Weirich, T.E.; Pischinger, S.; et al. Composition/Performance Evaluation of Lean NOx Trap Catalysts for Coupling with SCR Technology. *ChemCatChem* **2021**, *50*, 2274. [CrossRef]
9. Dupré, J.; Bazin, P.; Marie, O.; Daturi, M.; Jeandel, X.; Meunier, F. Effects of temperature and rich-phase composition on the performance of a commercial NOx-Storage-Reduction material. *Appl. Catal. B Environ.* **2016**, *181*, 534–541. [CrossRef]
10. Epling, W.S.; Campbell, L.E.; Yezerets, A.; Currier, N.W.; Parks, J.E. Overview of the Fundamental Reactions and Degradation Mechanisms of NOx Storage/Reduction Catalysts. *Catal. Rev.* **2004**, *46*, 163–245. [CrossRef]
11. Abdulhamid, H.; Fridell, E.; Skoglundh, M. The reduction phase in NOx storage catalysis: Effect of type of precious metal and reducing agent. *Appl. Catal. B Environ.* **2006**, *62*, 319–328. [CrossRef]
12. Amberntsson, A.; Fridell, E.; Skoglundh, M. Influence of platinum and rhodium composition on the NOx storage and sulphur tolerance of a barium based NOx storage catalyst. *Appl. Catal. B Environ.* **2003**, *46*, 429–439. [CrossRef]
13. Breen, J.P.; Burch, R.; Fontaine-Gautrelet, C.; Hardacre, C.; Rioche, C. Insight into the key aspects of the regeneration process in the NOx storage reduction (NSR) reaction probed using fast transient kinetics coupled with isotopically labelled 15NO over Pt and Rh-containing Ba/Al_2O_3 catalysts. *Appl. Catal. B Environ.* **2008**, *81*, 150–159. [CrossRef]
14. Olsson, L.; Westerberg, B.; Persson, H.; Fridell, E.; Skoglundh, M.; Andersson, B. A Kinetic Study of Oxygen Adsorption/Desorption and NO Oxidation over Pt/Al_2O_3 Catalysts. *J. Phys. Chem. B* **1999**, *103*, 10433–10439. [CrossRef]
15. Olsson, L.; Fridell, E. The Influence of Pt Oxide Formation and Pt Dispersion on the Reactions $NO_2 \Leftrightarrow NO+1/2\ O_2$ over Pt/Al_2O_3 and $Pt/BaO/Al_2O_3$. *J. Catal.* **2002**, *210*, 340–353. [CrossRef]
16. Bhatia, D.; McCabe, R.W.; Harold, M.P.; Balakotaiah, V. Experimental and kinetic study of NO oxidation on model Pt catalysts. *J. Catal.* **2009**, *266*, 106–119. [CrossRef]
17. Trovarelli, A. *Catalysis by Ceria and Related Materials*; Imperial College Press: London, UK, 2005; ISBN 1860942997.
18. Bunluesin, T.; Gorte, R.J.; Graham, G.W. Studies of the water-gas-shift reaction on ceria-supported Pt, Pd, and Rh: Implications for oxygen-storage properties. *Appl. Catal. B Environ.* **1998**, *15*, 107–114. [CrossRef]
19. Phatak, A.A.; Koryabkina, N.; Rai, S.; Ratts, J.L.; Ruettinger, W.; Farrauto, R.J.; Blau, G.E.; Delgass, W.N.; Ribeiro, F.H. Kinetics of the water–gas shift reaction on Pt catalysts supported on alumina and ceria. *Catal. Today* **2007**, *123*, 224–234. [CrossRef]
20. Pereda-Ayo, B.; De La Torre, U.; González-Marcos, M.P.; González-Velasco, J.R. Influence of ceria loading on the NOx storage and reduction performance of model $Pt–Ba/Al_2O_3$ NSR catalyst. *Catal. Today* **2015**, *241*, 133–142. [CrossRef]
21. Ji, Y.; Toops, T.J.; Crocker, M. Effect of Ceria on the Storage and Regeneration Behavior of a Model Lean NOx Trap Catalyst. *Catal. Lett.* **2007**, *119*, 257–264. [CrossRef]
22. Zhang, Y.; Yu, Y.; He, H. Oxygen vacancies on nanosized ceria govern the NOx storage capacity of NSR catalysts. *Catal. Sci. Technol.* **2016**, *6*, 3950–3962. [CrossRef]
23. Constantinou, C.; Li, W.; Qi, G.; Epling, W.S. NO_X storage and reduction over a perovskite-based lean NOX trap catalyst. *Appl. Catal. B Environ.* **2013**, *134–135*, 66–74. [CrossRef]

24. López-Suárez, F.E.; Illán-Gómez, M.J.; Bueno-López, A.; Anderson, J.A. NOx Storage reduction on a SrTiCuO3 perovskite catalyst studied by operando DRIFTS. *Appl. Catal. B Environ.* **2011**, *104*, 261–267. [CrossRef]
25. Ander Onrubia-Calvo, J.; Pereda-Ayo, B.; De-La-Torre, U.; Ramón González-Velasco, J. Perovskite-Based Formulations as Rival Platinum Catalysts for NO x Removal in Diesel Exhaust Aftertreatment. In *Perovskite Materials, Devices and Integration*; He, T., Ed.; IntechOpen: London, UK, 2019.
26. Wen, W.; Wang, X.; Jin, S.; Wang, R. $LaCoO_3$ perovskite in $Pt/LaCoO_3$ /K/Al_2O_3 for the improvement of NOx storage and reduction performances. *RSC Adv.* **2016**, *6*, 74046–74052. [CrossRef]
27. Fornasari, G.; Trifirò, F.; Vaccari, A.; Prinetto, F.; Ghiotti, G.; Centi, G. Novel low temperature NO storage-reduction catalysts for diesel light-duty engine emissions based on hydrotalcite compounds. *Catal. Today* **2002**, *75*, 421–429. [CrossRef]
28. Li, Q.; Meng, M.; Xian, H.; Tsubaki, N.; Li, X.; Xie, Y.; Hu, T.; Zhang, J. Hydrotalcite-derived $MnxMg_3$-xAlO catalysts used for soot combustion, NOx storage and simultaneous soot-NOx removal. *Environ. Sci. Technol.* **2010**, *44*, 4747–4752. [CrossRef]
29. Yu, J.J.; Jiang, Z.; Zhu, L.; Hao, Z.P.; Xu, Z.P. Adsorption/desorption studies of NOx on well-mixed oxides derived from Co-Mg/Al Hydrotalcite-like compounds. *J. Phys. Chem. B* **2006**, *110*, 4291–4300. [CrossRef]
30. Silletti, B.A.; Adams, R.T.; Sigmon, S.M.; Nikolopoulos, A.; Spivey, J.J.; Lamb, H.H. A novel Pd/MgAlOx catalyst for NOx storage-reduction. *Catal. Today* **2006**, *114*, 64–71. [CrossRef]
31. Fornasari, G.; Glöckler, R.; Livi, M.; Vaccari, A. Role of the Mg/Al atomic ratio in hydrotalcite-based catalysts for NOx storage/reduction. *Appl. Clay Sci.* **2005**, *29*, 258–266. [CrossRef]
32. Mahzoul, H.; Limousy, L.; Brilhac, J.F.; Gilot, P. Experimental study of SO2 adsorption on barium-based NOx adsorbers. *J. Anal. Appl. Pyrol.* **2000**, *2000*, 179–193. [CrossRef]
33. Westerberg, B.; Fridell, E. A transient FTIR study of species formed during NOx storage in the $Pt/BaO/Al_2O_3$ system. *J. Mol. Catal. A Chem.* **2000**, *2001*, 249–263.
34. Forzatti, P.; Castoldi, L.; Nova, I.; Lietti, L.; Tronconi, E. NOx removal catalysis under lean conditions. *Catal. Today* **2006**, *117*, 316–320. [CrossRef]
35. Nova, I.; Costaldi, L.; Lietti, L.; Tronconi, E.; Forzatti, P.; Prinetto, F.; Ghiotti, G. NOx adsorption study over Pt–Ba/alumina catalysts: FT-IR and pulse experiments. *J. Catal.* **2004**, *222*, 377–388. [CrossRef]
36. Dupré, J.; Bazin, P.; Marie, O.; Daturi, M.; Jeandel, X.; Meunier, F. Understanding the storage function of a commercial NOx-storage-reduction material using operando IR under realistic conditions. *Appl. Catal. B Environ.* **2014**, *160–161*, 335–343. [CrossRef]
37. Shi, C.; Ji, Y.; Graham, U.M.; Jacobs, G.; Crocker, M.; Zhang, Z.; Wang, Y.; Toops, T.J. NOx storage and reduction properties of model ceria-based lean NOx trap catalysts. *Appl. Catal. B Environ.* **2012**, *119–120*, 183–196. [CrossRef]
38. Sedlmair, C.; Seshan, K.; Jentys, A.; Lercher, J.A. Elementary steps of NOx adsorption and surface reaction on a commercial storage–reduction catalyst. *J. Catal.* **2003**, *214*, 308–316. [CrossRef]
39. Laible, T.; Pischinger, S.; Holderbaum, B. Internal and External Measures for Catalyst Light-Off Support. In *SAE Technical Paper Series. Proceedings of the 12th International Conference on Engines & Vehicles, Capri, Italy, 13 September 2015*; SAE International: Warrendale, PA, USA, 2015.
40. Jabłońska, M.; Wolkenar, B.; Beale, A.M.; Pischinger, S.; Palkovits, R. Comparison of Cu-Mg-Al-Ox and Cu/Al_2O_3 in selective catalytic oxidation of ammonia (NH_3-SCO). *Catal. Commun.* **2018**, *110*, 5–9. [CrossRef]
41. Wolkenar, B.; Schönebaum, S.; Mauermann, P.; Dittmann, P.; Pischinger, S.; Simon, U. Storage and Oxidation of Oxygen-Free and Oxygenated Hydrocarbons on a Pt–Pd Series Production Oxidation Catalyst. *Top. Catal.* **2019**, *62*, 376–385. [CrossRef]
42. Özyalcin, C.; Mauermann, P.; Dirkes, S.; Thiele, P.; Sterlepper, S.; Pischinger, S. Investigation of Filtration Phenomena of Air Pollutants on Cathode Air Filters for PEM Fuel Cells. *Catalysts* **2021**, *11*, 1339. [CrossRef]